

Characterizing elastic turbulence in channel flows at low Reynolds number

Boqiang Qin and Paolo E. Auliana

*Department of Mechanical Engineering and Applied Mechanics, University of Pennsylvania,
Philadelphia, Pennsylvania 19104, USA*

(Received 14 September 2016; published 10 April 2017)

We present an investigation of a fully developed, steady, parallel channel flow at low Reynolds number. As the Reynolds number becomes sufficiently small, the flow becomes unstable to nonlinear, bifurcated, chaotic, and aperiodic motion, even though the flow is laminar and the geometry is simple. Using the same experimental setup, we compare the flow in the case of a smooth channel, which is a typical example of parallel channel flow; and in the case of a rough channel, which is a typical example of parallel channel flow with rough walls. We propose a simple mechanism to explain the growth of vorticity in parallel channel flow based on polymer stretching and contraction in the case of elastic turbulence.

DOI: 10.1103/PhysRevFluids.2.083302

I. INTRODUCTION

Unlike the case of fully developed, steady, parallel channel flow, chaotic motion can exhibit itself in the absence of inertia, i.e., at low Reynolds number (Re) [1–8]. A high order of chaos, of fully developed, steady, parallel channel flow exhibits a complete difference of chaotic behavior, elasticity, bifurcation, and chaos in Newtonian liquid [9–12]. Parallel channel flow in the absence of inertia, in many practical cases, and understanding the underlying fundamental physics of how chaotic motion (e.g., blood, cells, and microorganisms) [13–16], chemical and polymer-induced chaotic motion have been playing a role in polymer science [17,18], and micro- and nanofluidic devices [11,19–21].

The emergence of chaotic motion in the case of parallel channel flow is a result of the development of polymer elastic effects in the flow, and the consequent change in polymer conformation in the flow. The effects are mainly dependent on the geometry, and depend on the nature of the flow [22]. Elastic effects are observed in the case of the mean flow, for instance, in the case of the flow in a rough channel [10,23,24], in the case of concentric channels [1,2,4,12], in a rough channel [11], and in a noncircular channel [5,25]. In the case of the mean flow, high-velocity gradients and curved streamlines can stretch the polymer molecules, inducing elastic effects and chaotic motion [22]. In fact, it has been argued that a necessary condition for nonlinear behavior to be amplified by the nonlocal imbalance in the fully developed flow [26–28] and much of recent work on elastic bifurcation has been devoted to geometry [9,25].

Recent theoretical investigations, however, have shown that fully developed, steady, parallel channel flow can be nonlinear, unstable even in parallel channel flow, in a straight pipe and channel at low Re [29–33]. For example, nonlinear behavior analysis [29–31] predicts a bifurcated bifurcation from stable behavior, while nonmodal stability analysis predicts an eigenvalue of positive growth rate of polymer stretching in small pipe [34] found, nevertheless, vorticity generation has a significant impact on the chaotic behavior (a characteristic of chaotic motion) [35] reported. Moreover, the existence of a nonlinear, bifurcated motion of fully developed, steady, parallel channel flow in a (micro)channel is reported in the present [8]. It is shown that, in the absence of inertia (i.e., at low Reynolds number), a nonlinear flow of polymer is expected to develop and the resulting chaotic motion is highly elastic [8]. This bifurcated motion in a fully developed channel flow is hence akin to the motion from laminar to turbulent flow of simple Newtonian liquid (e.g., water) in pipe, except that the

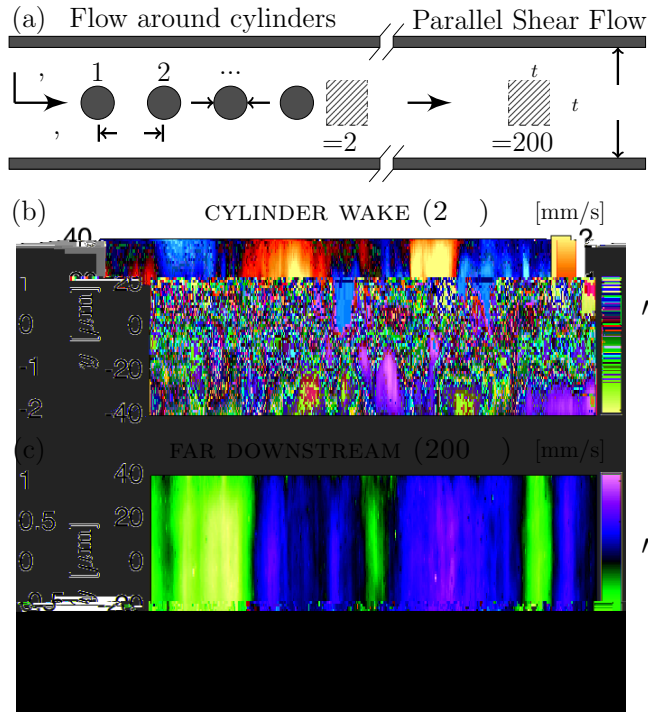


FIG. 1. (a) Schematic of the experimental channel geometry. (b) Space-time plot of the streamwise velocity fluctuations, u' , immediately after the last cylinder, for $x = 2W$ and $Wi = 10$. (c) The streamwise velocity fluctuations far downstream at $200W$.

going parameter is the Weissenberg number (Wi), defined as the product of the relaxation time λ and the shear rate $\dot{\gamma}$. However, the main feature of the elongational flow is to be fully characterized and analyzed, the oscillatory flow in a high channel remains poorly understood.

In this paper, we investigate the flow of a polymer fluid in a high microchannel using particle tracking method. The oscillatory flow is characterized and monitored (i) immediately after the last cylinder and (ii) far downstream. We find that both the oscillations on the cylinder and far downstream have a similar feature, including velocity fluctuations, characteristic time scales and partial length scales. The effective, however, significant difference between the oscillations including the velocity fluctuations, characteristic time scales, and partial and partial period. A simple mechanism is proposed for the sustained velocity fluctuations in the parallel shear flow region based on a self-sustaining mechanism of energy feedback between the velocity fluctuations and polymer elastic energy.

II. METHODS

The flow of a dilute polymer solution in a high microchannel with a quarter section ($W = D = 100 \mu\text{m}$). The microchannel is made of polydimethylsiloxane using standard soft-lithography method. The length of the microchannel is much larger than the channel width $W = 330$ and is divided into two regions. The region is composed of a line of cylinders with a length of $30W$. A total of 15 cylinders ($n = 15$) is placed in the line as a schematic is shown in Fig. 1(a). Each cylinder has a diameter d of $0.5W$ and is evenly spaced with

a separation of $= 2W$; the last cylinder is at position $x = 0$. The second region is a long parallel shear flow, which follows the initial linear array of cylinders and is $200W$ length. More details on the channel design can be found elsewhere [8].

The polymeric solution is prepared by adding 300 ppm of polyacrylamide (PAA) (108 MW) in a viscous Newtonian solvent (90% by weight glycerol aqueous solution); the PAA polymer overlap concentration (c^*) is approximately 350 ppm [5] and $c/c^* = 0.86$. This polymeric solution possesses a nearly constant viscosity of approximately 200 mPa s; for more information on the rheological properties of the fluid, see the Supplemental Material and [8]. A Newtonian solution, 90% by weight glycerol in water, is also used for comparison. The Reynolds number is kept below 0.01, where $Re = UH/\nu$, U is the mean centerline velocity, H is the channel half-width, and ν is the fluid density. The strength of the elastic stresses compared to viscous stresses is characterized by the Weissenberg number [17], here defined as $Wi = N_1(\dot{\gamma})/2\dot{\gamma}(\dot{\gamma})$, where $\dot{\gamma} = U/H$ is the shear rate and N_1 is the first normal stress difference. The fluid relaxation time is obtained from shear rheology data (see [6]) and is defined as $\lambda = N_1(\dot{\gamma})/2\dot{\gamma}^2$; values of λ range from 0.1 to 1.0 s for the typical shear rates in the channel experiment. For the experiments presented here, the Weissenberg number is kept constant at approximately 10 and the number of cylinders at 15. We note that the critical value of Wi for the onset of the critical instability in the parallel flow region is $Wi_c = 5.2$ for the type of disturbances (15 cylinders) introduced here [6].

The flow is characterized using particle tracking velocimetry. Fluorescent particles (10 μ m diameter) are dispersed in the fluids and imaged using an epifluorescent microscope and a high-speed camera (up to 10 frames/s). Spatially resolved velocity fields are obtained by tracking particles in a rectangular window (width equal to $0.9W$, length equal to $0.2W$, and centered at $x = 0$) with a grid resolution of 1μ m. The resultant time resolution is $\Delta t = 25$ ms. However, we can increase the time resolution and duration of the velocimetry measurements by decreasing the window size (width equal to $0.1W$ and length to $0.7W$). This time-resolved measurement produces velocity time series with high resolution ($\Delta t = 1$ ms) and relatively long sampling duration (up to 300 s).

III. RESULTS AND DISCUSSION

We begin our flow analysis by measuring the flow streamwise velocity, $u(x, y, t)$ in the wake of the last cylinder ($x = 2W$) as well as in the parallel shear region ($x = 200W$) using the spatially resolved measurement (i.e., large window size). The streamwise velocity fluctuations are obtained by subtracting the ensemble average from the measured signal $u = \bar{u} + \delta u$. Figure 1(b) shows the space time plot of $\delta u(y, t)$ along a cut line in the wall-normal direction (y axis) at the cylinder wake region [$x = 2W$ in Fig. 1(a)] of the channel. Here the spatial coordinate used is the wall-normal coordinate and the channel centerline is at 0. The data show relatively large velocity fluctuations in the cylinder wake, with the amplitude reaching approximately 28% of the overall channel centerline mean speed (7 mm/s). Along the y direction, we find that high-intensity fluctuations are concentrated in the form of spots, which are manifestations of streamwise streaks of high- and low-local-velocity fluctuations. These streaks have a wide range of temporal durations and spatial sizes, as large as the cylinder diameter (50 μ m) and as small as the velocity grid spacing (1 μ m). Far downstream [200; see Fig. 1(c)], however, the flow is significantly different from that in the cylinder wake. We find that velocity fluctuations at 200 exist in the form of aperiodic bursts of various durations and appear to be spatially smoother in the wall-normal direction. We note that no appreciable fluctuations are found in the Newtonian case under similar conditions. Overall, we find markedly different flow structures as the fluid moves from regions near the cylinder (curved flows) to the parallel shear region.

To quantify the temporal dynamics of the (unstable) flow, we measure the centerline velocity fluctuations $u_c(t)$ for both Newtonian and polymeric solutions in the wake of the cylinder [Fig. 1(b)] and in the parallel shear region [Fig. 1(c)] using the small interrogation window. The data show significant velocity fluctuations for the viscoelastic fluid; the standard deviation (i.e., fluctuations) reaches approximately 10% of the centerline mean, in both regions of the flow. No significant

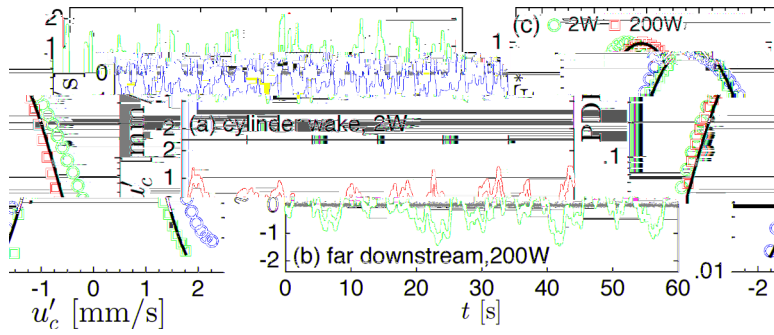
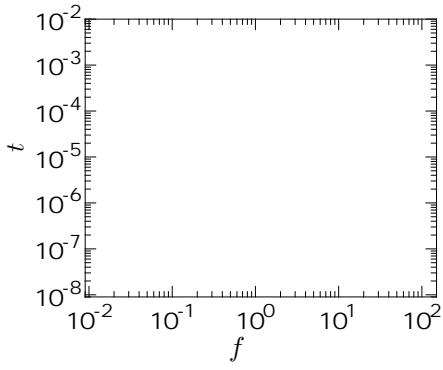


FIG. 2. Time series and the associated probability distribution of center line velocity fluctuations u'_c for n

CHARACTERIZING ELASTIC TURBULENCE IN CHANNEL ...



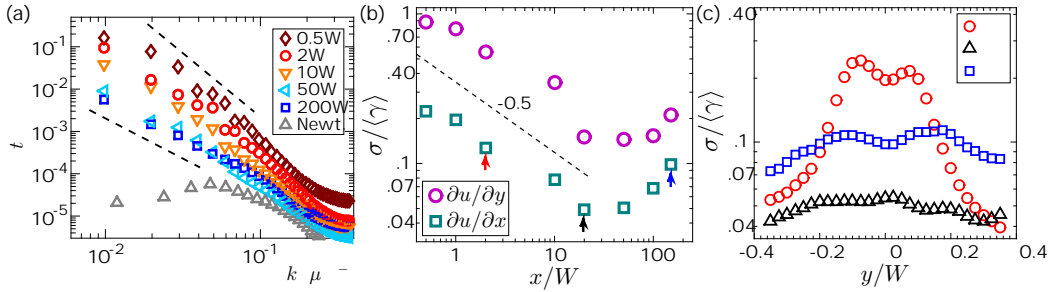


FIG. 4. Spatial characteristics of the (inertial) velocity field along the channel for $Wi = 10$ and $n = 15$. (a) Spatial power spectrum as a function of wavenumber k (parallel to the flow direction) of the velocity, u , averaged along the channel position. (b) The magnitude σ of the transverse and longitudinal components of the velocity gradient, normalized by the parallel mean shear rate $\langle \dot{\gamma} \rangle$ in the parallel shear flow. (c) Longitudinal component of the momentum autocorrelation function immediately in the channel (20W), at the end of the channel (50W), and far downstream in the parallel shear flow (150W).

direction is orthogonal to the mean flow and provide insight into the u , v , w in the direction of gradient in shear. We find that the u is associated with a wide range of parallel length scale l (from $100 \mu\text{m}$ down to approximately $5 \mu\text{m}$) in the all-noise direction and has a parallel variation in u a few micrometers near the surface of the channel than in the parallel shear region [see also Fig. 1(b) and 1(c)]. The parallel spectrum of the velocity near the channel follows a k^{-3} decay. Note that the wavenumber k is the inverse of l , which is the parallel wavenumber. At the end of the channel, the parallel u is weakened, and the spectrum follows k^{-2} ; the data at the end of the channel are almost identical to the channel [see Fig. 1(c)]. The u along the channel is shown in Fig. 3(a), indicating that the u near the channel and in the parallel shear region provide a clear picture of elastic behavior, the u is quite different in u , v , w . This shows the difference between elastic behavior in u in the eddy geometry and in a single channel in a single flow.

So far, we have shown that the u of a polymer is different in a parallel shear geometry, mainly due to the large velocity gradient in both space and time even at low Re . The velocity gradient, far downstream from the initial perturbation, is most likely due to the stretching of polymer molecules in the u . To establish this point, we measure the root-mean-square (rms) variation of the shear rate ($\dot{\gamma}$) and longitudinal ($\dot{\gamma}_x$) components of the velocity gradient; here the rms of quantity A is defined as $\sigma = (A - \langle A \rangle)^2$, similar to [39]. The components (quantity) are known to measure the stretching in random flow [39–42].

Figure 4(b) shows the magnitude σ of $\dot{\gamma}_x$ and $\dot{\gamma}_y$ as a function of position along the channel normalized by the parallel average shear rate $\langle \dot{\gamma} \rangle$ downstream in the parallel shear flow. Near the surface of the channel, $\dot{\gamma}_x$ and $\dot{\gamma}_y$ can be compared to the velocity gradient elastic behavior in the parallel shear flow. Moreover, the $\dot{\gamma}_x$ component dominates $\dot{\gamma}_y$ and both components decay as the polymer solution u downstream. The end point is downstream approximately 20W in the channel. However, at $x = 20W$, $\dot{\gamma}_x$ and $\dot{\gamma}_y$ both components of $\sigma/\langle \dot{\gamma} \rangle$ end and begin to increase as the u downstream. Consequently, the u behavior has the v , w in the longitudinal component become increasingly comparable to that of the shear component. The end clearly shows a change in u at around 20W accompanied by an increase in velocity gradient and polymer stretching. This non-monotonic end is also captured by plotting the parallel profile of $\sigma/\langle \dot{\gamma} \rangle$ for $\dot{\gamma}_x$ across the channel and $\dot{\gamma}_y$ (y axis) for the different channel location, shown in Fig. 4(c). The data suggest that polymer molecules are increasingly stretched by the gradient in the u and v direction beyond 20W.

To further demonstrate that the magnitude of the fluctuation in velocity gradients is large enough to generate polymer stretching, we compute a Weissenberg number based on fluctuations in the velocity gradients. Here $Wi_{rms} = (\dot{u})_{rms} (\lambda / y)$, where the rms fluctuation of the shear gradient is nondimensionalized by the polymer relaxation time. Using the relaxation time corresponding to $Wi = 10.2$, we find that $Wi_{rms} = 5.2$ in the cylinder wake ($x = 2W$), while far downstream, it is approximately 2. Moreover, far downstream, the Weissenberg number based on the rms of elongational $Wi_{rms}^e = 1$. We note that the values of both Wi_{rms} and Wi_{rms}^e are near or larger than 1, which suggests that the flow is able to generate sufficient polymer stretching.

IV. CONCLUSION

In summary, we investigated the flow of a viscoelastic fluid in a parallel shear geometry at low Re. This flow becomes unstable via a nonlinear subcritical instability above a critical Weissenberg number ($Wi_c = 5.2$) if perturbations are strong enough. [Using spatially and temporally resolved velocimetry, we identified signatures of elastic turbulence in the parallel shear region. This flow contrasts in many ways with elastic turbulence near the array of cylinders, which we had found in our previous experiments (same experimental setup) to be linearly unstable. Specifically, we found that the flow near cylinders is organized by streamwise streaks that manifest as spots in Fig. 1(b), while temporal bursts that manifest as spanwise bands are found in the parallel shear region [Fig. 1(c)]. Moreover, the energy contained in the high-frequency range near the cylinders seems to shift toward the low-frequency range in the parallel shear region [Fig. 1(d)]. We provided a simple mechanism for the sustained (and even growth) of velocity fluctuations in the parallel shear region (

- [10] A. G. G. Oei and V. S. Eisele, Elastic triblends in a polymer solution, *Journal of Polymer Science* (London) **405**, 53 (2000).
- [11] A. G. G. Oei and V. S. Eisele, Efficient mixing of a low molecular weight polymer in a polymer solution, *Journal of Polymer Science* (London) **410**, 905 (2001).
- [12] M. A. Fardin, D. Lopez, J. C. Ochoa, G. G. G. Oei, O. Cardoso, G. H. McKinley, and S. Leroy, Elastic triblends in Shear-Banding Wormlike Micelles, *Physical Review Letters* **104**, 178303 (2010).
- [13] R. G. Henke, R. E. A. K. Sinha, and M. D. Graham, Malignant Regime and Drainage Transition in Connected Micellar Components Separation, *Physical Review Letters* **114**, 188101 (2015).
- [14] M. Thiabaud, Z. Shen, J. Huang, and C. Michard, Prediction of Anomalous Blood Viscosity in Connected Shear Flow, *Physical Review Letters* **112**, 238304 (2014).
- [15] M. L. E. and V. S. Eisele, Complex Dynamics of Composed Viscosity in Linear Flow, *Physical Review Letters* **112**, 138106 (2014).
- [16] S. G. Li, D. Liepmann, and S. J. M. L. E., Elastic second-order of emulsion DNA solution in a 90° microworld, *Physical Review E* **78**, 036314 (2008).
- [17] B. M. Lennox, C. S. O. M., V. B. O. A., C. W. A., D. B. O., and W. S. A., Intrinsic Role of Melting in Polymer Electrolyte: A Weakly Nonlinear Subcritical Instability of Viscoelastic Poiseuille Flow, *Physical Review Letters* **90**, 024502 (2003).
- [18] M. M. Denn, Features of non-Newtonian fluid dynamics, *AIChE Journal* **50**, 2335 (2004).
- [19] J. Zilberstein, R. J. Poole, M. A. Alejo, D. B. O., B. L. A., and A. Lindner, Geometric scaling of a parallel elastic instability in a pipe channel, *Journal of Fluid Mechanics* **712**, 203 (2012).
- [20] Y. C. Lam, H. Y. Gan, N.-T. Nguyen, and H. L. E., Microemulsion-based viscoelastic instability at low Reynolds number, *Biomicrofluidics* **3**, 014106 (2009).
- [21] C. Scholten, F. W. G., J. R. Gomez-Solano, and C. Bechinger, Enhanced dipole interaction between elastic triblends in porous media, *Biophysical Letters* **107**, 54003 (2014).
- [22] R. G. Larson, *The Structure and Rheology of Complex Fluids* (Oxford University Press, New York, 1999), Vol. 33.
- [23] T. B. Ghelea, E. Segre, and V. S. Eisele, Elastic triblends in a Karmann-Klingenberg-Green-Goldstick, *Physical Fluids* **19**, 053104 (2007).
- [24] Y. J. N. and V. S. Eisele, Poiseuille and Poiseuille flow in elastic triblends over a wide range of polymer concentration, *Physical Review Letters* **102**, 124503 (2009).
- [25] M. Gilli, A. V. Q. E. -Q. E. A., and M. E. L. O., Transition to triblends and mixing in a viscoelastic fluid flowing in a channel with a periodic array of cylindrical obstacles, *Physical Review Letters* **110**, 174501 (2013).
- [26] G. H. McKinley, P. Pakdel, and A. A. Ekin, Rheological and geometric scaling of parallel elastic instability, *Journal of Non-Newtonian Fluid Mechanics* **67**, 19 (1996).
- [27] P. Pakdel and G. H. McKinley, Elastic instability and curved streamlines, *Physical Review Letters* **77**, 2459 (1996).
- [28] E. S. G. Shaqfeh, Parallel elastic instability in a microfluidic system, *Annual Review of Fluid Mechanics* **28**, 129 (1996).
- [29] B. M. Lennox, C. S. O. M., A. N. M. O. O., and W. S. A., Weakly nonlinear subcritical instability of viscoelastic Poiseuille flow, *Journal of Non-Newtonian Fluid Mechanics* **116**, 235 (2004).
- [30] A. N. M. O. O. and W. S. A., Subcritical Finite-Amplitude Solution for Plane Couette Flow of Viscoelastic Fluid, *Physical Review Letters* **95**, 024501 (2005).
- [31] A. N. M. O. O. and W. S. A., An inhomogeneous subcritical instability and the transition to triblends in viscoelastic parallel shear flow, *Physical Review Letters* **447**, 112 (2007).
- [32] M. R. Johnson and S. Kumar, Transition to chaos in a viscoelastic flow, *Physical Fluids* **22**, 023101 (2010).
- [33] M. R. Johnson and S. Kumar, Nonmodal amplification of chaotic disturbances in a viscoelastic channel flow, *Journal of Non-Newtonian Fluid Mechanics* **166**, 755 (2011).
- [34] D. Bonn, F. Ingremeau, Y. Amaral, and H. Kella, Lagrangian dynamics in a microfluidic pipe flow of polymer solution, *Physical Review E* **84**, 045301 (2011).
- [35] E. Pelletier, C. Viehke, J. Meadows, and P. A. Williams, Dilute polymer lamellar solution, dendritic ensembles, *Langmuir* **19**, 559 (2003).

- [36] See Supplemental Material at <http://link.aps.org/supplemental/10.1103/PhysRevFluids.2.083302> for details on rheology and experimental method.
- [37] J. J. Magda, C. S. Lee, S. J. M. Little, and R. G. Larson, Rheology, viscoelasticity, and heat-induced diffusion in polymer entanglement, *Macromolecules* **26**, 1696 (1993).
- [38] T. B. Ghelea, E. Segre, and V. Steinberg, Role of Elastic Stress in Statistical and Scaling Properties of Elastic Turbulence, *Phys. Rev. Lett.* **96**, 214502 (2006).
- [39] Y. Li and V. Steinberg, Shearing of polymer in a random flow: Effect of a heat source, *Exp. Fluids* **90**, 44005 (2010).
- [40] E. Balkoň, A. Fofon, and V. Lebedev, Turbulent Dynamics of Polymer Solution, *Phys. Rev. Lett.* **84**, 4765 (2000).
- [41] M. Cheko, Polymer Shearing by Turbulence, *Phys. Rev. Lett.* **84**, 4761 (2000).
- [42] S. Geachenko and V. Steinberg, Critical long distance in polymer dynamics near the coil-stretch transition in elongational flow, *Phys. Rev. E* **78**, 040801 (2008).
- [43] T. T. Pe kin, D. E. Smi h, and S. Chř, Single polymer dynamics in an elongational flow, *Science* **276**, 2016 (1997).
- [44] D. E. Smi h, H. P. Babcock, and S. Chř, Single-polymer dynamics in steady shear flow, *Science* **283**, 1724 (1999).